THE ASTRONOMICAL JOURNAL VOLUME 85, NUMBER 8 AUGUST 1980

THE RESONANCE OVERLAP CRITERION AND THE ONSET OF STOCHASTIC BEHAVIOR IN THE RESTRICTED THREE-BODY PROBLEM[a)]

JACK WISDOM
California Institute of Technology, Pasadena, California 91125
Received 19 February 1980; revised 22 April 1980

ABSTRACT

The resonance overlap criterion for the onset of stochastic behavior is applied to the planar circular-restricted three-body problem with small mass ratio (μ). Its predictions for $\mu = 10^{-3}$, 10^{-4}, and 10^{-5} are compared to the transitions observed in the numerically determined Kolmogorov-Sinai entropy and found to be in remarkably good agreement. In addition, an approximate scaling law for the onset of stochastic behavior is derived.

I. INTRODUCTION

Is the solar system stable? There is as yet no answer to this notoriously difficult question, but some important steps have been made in the study of the stability of dynamical systems in the last two decades. Hénon and Heiles (1964) discovered in their now-classic study that the phase space of a simple nonlinear Hamiltonian system with two degrees of freedom (a model for the motion of stars in the Galaxy) was divided into regions that contain quasiperiodic trajectories and regions in which trajectories have a random character. Subsequent numerical experiments by Hénon (1966), Bozis (1966), and Jefferys (1966) then verified that the phase space of the planar circular-restricted three-body problem is similarly divided. The existence of regions of quasiperiodic trajectories is very important since all such trajectories possess long-term stability. While there is no rigorous way of predicting which regions will be stochastic, an approximate criterion involving the overlap of zero-order nonlinear resonances has been developed which has had considerable success in other problems (see Walker and Ford 1969 and the recent review in Chirikov 1979). The solar system is far too complicated, though, for a direct application of the resonance overlap criterion. To get our foot in the door of dynamical astronomy and gain confidence in the overlap criterion, I begin instead with the simplest of unsolved problems in dynamical astronomy. In this paper I apply the resonance overlap criterion to the planar circular-restricted three-body problem and compare its results to some numerical experiments.

In Sec. II, I review the resonance overlap criterion. I then apply the method to the restricted three-body problem in Sec. III. A comparison of its predictions with some numerical experiments is presented in Sec. IV. In Sec. V, I derive an approximate scaling law for resonance overlap, and in Sec. VI, I state my conclusions.

II. RESONANCE OVERLAP AND THE CHIRIKOV CRITERION

Consider a Hamiltonian of the form

$$H = H_0(J_1,J_2) + \mu \sum_{i=0}^{\infty} \sum_{j=-\infty}^{\infty} \times H_{ij}(J_1,J_2)\cos(i\theta_1 + j\theta_2), \quad (1)$$

where θ_l are the coordinates canonically conjugate to the momenta J_l and μ is a small parameter. One may attempt to solve this problem by first solving the zero-order Hamiltonian

$$H^{(0)}_{nm} = H_0(J_1,J_2) + \mu \sum_{k=0}^{\infty} \times H_{kn,km}(J_1,J_2)\cos[k(n\theta_1 + m\theta_2)] \quad (2)$$

and then perturbing the zero-order solutions with the remaining terms. This zero-order Hamiltonian will be useful whenever the resonance condition

$$n\omega_1(J_1,J_2) + m\omega_2(J_1,J_2) = 0 \quad (3)$$

is approximately satisfied, where

$$\omega_l(J_1,J_2) \equiv \frac{\partial(H_0 + \mu H_{00})}{\partial J_l}, \quad (4)$$

since the arguments of the cosines will then be approximately stationary. I assume n and m have no common divisors. In terms of the resonance variables

$$\psi = n\theta_1 + m\theta_2$$

and (5)

$$\varphi = -\theta_2/n,$$

this Hamiltonian assumes the simpler form

$$H^{(0)}_{nm} = H'_0(\Phi,\Psi) + \mu \sum_{k=0}^{\infty} H'_{kn,km}(\Phi,\Psi)\cos k\psi, \quad (6)$$

where

$$\Psi = J_1/n$$

[a)] Contribution No. 3390 of the Division of Geological and Planetary Sciences, California Institute of Technology, Pasadena, California 91125.

0004-6256/80/081122-12$00.90

and

$$\Phi = mJ_1 - nJ_2 \tag{7}$$

are the momenta canonically conjugate to ψ and φ, respectively. Since $H^{(0)}_{nm}$ has no explicit time dependence and is cyclic in φ, the system has two integrals of the motion, the Hamiltonian itself and Φ. Liouville's theorem (see Whittaker 1961) then guarantees that there is a canonical transformation to the system in which these integrals are the new momenta and the new Hamiltonian

$$\tilde{H}^{(0)}_{nm} = \tilde{H}^{(0)}_{nm}(H^{(0)}_{nm}, \Phi) \tag{8}$$

is cyclic in the new coordinates and thus trivially integrable. The character of the solutions is, however, most easily obtained by studying the contours of $H^{(0)}_{nm}$ on surfaces of constant Φ. To illustrate this, I make three simplifying assumptions. The first two are that we can ignore $H'_{kn,km}$ for all k except $k = 1$ and that $H'_{n,m}(\Phi,\Psi)$ is sufficiently well approximated near the resonance by $H'_{n,m}(\Phi,\Psi_R)$, where Ψ_R is defined implicitly by the resonance condition

$$\omega_\psi(\Phi,\Psi_R) \equiv \frac{\partial H'_0(\Phi,\Psi)}{\partial\Psi}\bigg|_{\Psi=\Psi_R} = 0. \tag{9}$$

The third simplifying assumption is that $H_0(\Phi,\Psi)$ is sufficiently well approximated by the quadratic terms in its Taylor series about $\Psi = \Psi_R$. Under these assumptions the resonance Hamiltonian is approximately

$$H^{(0)}_{nm} \simeq H'_0(\Phi,\Psi_R) + \frac{1}{2}\frac{\partial^2 H'_0}{\partial\Psi^2}\bigg|_{\Psi=\Psi_R} \times (\Psi - \Psi_R)^2 + \mu H'_{n,m}(\Phi,\Psi_R)\cos\psi, \tag{10}$$

where the linear term is absent because of the resonance condition (9). The level curves of this approximate $H^{(0)}_{n,m}$ are then explicitly

$$\Psi = \Psi_R \pm \left(\frac{H^{(0)}_{nm} - H'_0(\Phi,\Psi_R) - \mu H'_{n,m}(\Phi,\Psi_R)\cos\psi}{\frac{1}{2}\frac{\partial^2 H'_0}{\partial\Psi^2}\Big|_{\Psi=\Psi_R}}\right)^{1/2}. \tag{11}$$

Figure 1 illustrates these contours in the Cartesian coordinates $x = (2\Psi)^{1/2}\cos\psi$ and $y = (2\Psi)^{1/2}\sin\psi$. In drawing this figure, I have assumed $H^{(0)}_{nm} - H'_0(\Phi,\Psi_R)$ and $H'_{n,m}(\Phi,\Psi_R)$ are opposite in sign, and have arbitrarily restricted Ψ to be greater than zero. The extremum at the origin is an artifact of this restriction. It is clear that if a contour does not enclose the origin, then the angle ψ oscillates, whereas if a contour encircles the origin, ψ circulates. The oscillation region has been shaded in Fig. 1. The contours that form the boundary of the oscillation region are the so-called separatrices, which play an important role in the resonance overlap criterion. For the approximate Hamiltonian (10) the separatrices are

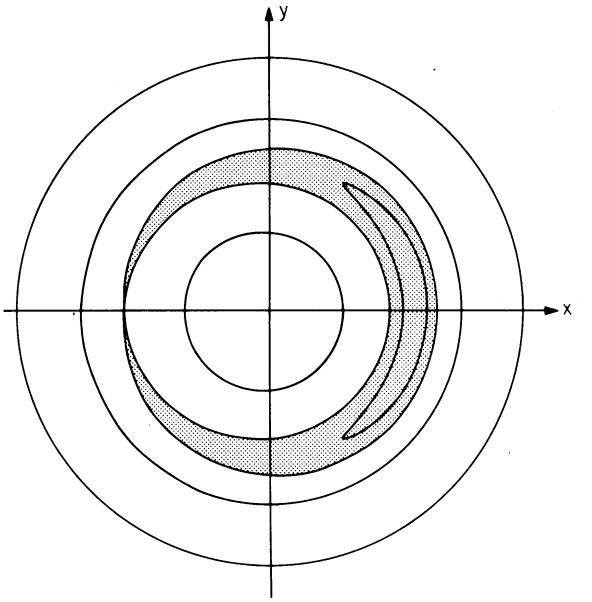

FIG. 1. Contours of the approximate Hamiltonian (10) on a surface of constant Φ. The Cartesian coordinates are $x = (2\Psi)^{1/2}\cos\psi$ and $y = (2\Psi)^{1/2}\sin\psi$.

$$\Psi_S = \Psi_R \pm \Delta\Psi\cos\frac{\psi}{2}, \tag{12}$$

where the resonance half-width $\Delta\Psi$ is defined by

$$\Delta\Psi \equiv 2\left(\frac{\mu H'_{n,m}(\Phi,\Psi_R)}{\frac{\partial^2 H'_0}{\partial\Psi^2}\Big|_{\Psi=\Psi_R}}\right)^{1/2}. \tag{13}$$

Now, if the three simplifying assumptions leading to the approximate Hamiltonian (10) are valid, the contours of the full resonance Hamiltonian (6) will be qualitatively the same as those in Fig. 1. For a more general Hamiltonian than that of Eq. (10), the contours can be quite different and require a detailed numerical mapping to determine the oscillation regions.

Having, in principle, completely solved the zero-order resonance Hamiltonian (6) by reducing it to the form of Eq. (8), I now ask what effect the other terms in the full Hamiltonian (1) will have on the unperturbed solutions. In the system with $H^{(0)}_{nm}$ and Φ as momenta, the full Hamiltonian has the form

$$H = \tilde{H}_{nm}(H^{(0)}_{nm}, \Phi) + \mu\sum_{i=0}^{\infty} \times \sum_{j=-\infty}^{\infty} \tilde{H}_{ij}(H^{(0)}_{nm}, \Phi)\cos(ih + j\varphi), \tag{14}$$

where h and φ are canonically conjugate to $H_{nm}^{(0)}$ and Φ, respectively. If the resonance conditions of this Hamiltonian analogous to the resonance condition (3) of the zero-order resonance Hamiltonian are sufficiently poorly satisfied and the H_{ij} are small enough, then the Kolmogorov-Arnol'd-Moser Theorem (see Moser 1973) assures us that the motion is still quasiperiodic and only slightly perturbed. On the other hand, if a second resonance of the original Hamiltonian is "sufficiently close," then the motion is more complicated. In fact, there has been no successful analytic attempt to solve for the motion under the simultaneous influence of two "close" resonances, nor is there a rigorous analytic estimate of what "sufficiently close" means. The basic idea of the resonance overlap criterion is that two resonances are "sufficiently close" when a separatrix of one resonance has crossed a separatrix of the other resonance, i.e., when the zero-order analysis indicates that two different resonance angles both oscillate. Ideally one would map all initial conditions in the four-dimensional phase space that lead to oscillation of each resonance angle and then look for the overlap of these regions. In practice, it is easier to specify initial values of θ_1 and θ_2 and then plot the separatrices for each resonance in the $J_1 - J_2$ plane. The simple example of Walker and Ford (1969) provides an excellent introduction to this method. Chirikov (see Chirikov 1979) has developed an approximate criterion. Chirikov first calculates the half-width of each resonance by Eq. (13), having made all three assumptions leading to the approximate Hamiltonian (10) and implicitly choosing θ_1 and θ_2 for each resonance to give the maximum width. He then calculates frequency half-widths by the approximate relation

$$\Delta\omega_I^q \simeq \left.\frac{\partial\omega_I}{\partial\Psi}\right|_{\Psi=\Psi_R} \Delta\Psi, \tag{15}$$

with the frequencies of Eq. (4). The superscript identifies the resonance under study. The half-widths of nearby resonances are then compared to the separation of the resonance centers,

$$\delta\omega_I^{qb} = |\omega_I^q - \omega_I^b|. \tag{16}$$

If both inequalities

$$\Delta\omega_1^q + \Delta\omega_1^b \geq \delta\omega_1^{qb}$$

and (17)

$$\Delta\omega_2^q + \Delta\omega_2^b \geq \delta\omega_2^{qb}$$

are satisfied, then there is resonance overlap. This then is Chirikov's approximate criterion. In Sec. III, I apply the resonance overlap criterion to the restricted three-body problem.

III. RESONANCE OVERLAP IN THE RESTRICTED THREE-BODY PROBLEM

In terms of the Delaunay canonical elements (see, e.g., Brouwer and Clemence 1961), the Hamiltonian for the planar circular-restricted three-body problem is

$$H = -\frac{(1-\mu)^2}{2L^2} - R, \tag{18}$$

where

$$R = \mu \sum_{i=0}^{\infty} \sum_{j=-\infty}^{\infty} K^{(i,j)} \cos N^{(i,j)} \tag{19}$$

and

$$N^{(i,j)} = il + j(t-g). \tag{20}$$

I have chosen units so that the product of the gravitational constant and the sum of the two masses is unity and the separation of the two masses is also unity. In these units the secondary has mass μ, which I assume is small compared to unity. In terms of the usual osculating elliptic elements, the canonical momenta are $L = [(1-\mu)a]^{1/2}$ and $G = [(1-\mu)a(1-e^2)]^{1/2}$, where a is the semimajor axis and e is the eccentricity. Their conjugate coordinates are the mean anomaly l and the angle of periapse g, respectively. $K^{(i,j)}$ is a function of L and G, and t is the time. A resonance occurs when one of the cosine arguments is nearly stationary. Since this Hamiltonian is time dependent, the resonance condition assumes a slightly different form,

$$0 = -s\omega_l(L,G) + (s+s')[1 - \omega_g(L,G)], \tag{21}$$

where s and s' are integers and the frequencies are defined in the usual way:

$$\omega_l \equiv \frac{\partial}{\partial L}\left(\frac{-(1-\mu)^2}{2L^2} - \mu K^{(0,0)}(L,G)\right)$$

and (22)

$$\omega_g \equiv \frac{\partial}{\partial G}[-\mu K^{(0,0)}(L,G)].$$

If we ignore the terms proportional to μ, we get the approximate resonance condition

$$0 = -s/L^3 + (s+s'), \tag{23}$$

or, in terms of the semimajor axis,

$$\alpha_{ss'} = [s/(s+s')]^{2/3}. \tag{24}$$

Poincaré (1902) was the first to study motion near a resonance in the restricted three-body problem by means of a zero-order resonance Hamiltonian of the type discussed in Sec. II. I perform a canonical transformation to the Poincaré resonance variables, as generalized by Woltjer (1923) and Hagihara (1943),

$$\varphi = l + g - t$$

and (25)

$$\psi = -sl + (s+s')(t-g)$$

via the generating function

$$F = [-sl + (s+s')(t-g)]\Psi + [l+g-t]\Phi. \tag{26}$$

Their respective conjugate momenta are

$$\Phi = \frac{(s+s')L - sG}{s'}$$

and (27)

$$\Psi = \frac{L-G}{s'}.$$

In terms of the osculating elliptic elements, these are

$$\Phi = [(1-\mu)a]^{1/2}\left(\frac{(s+s') - s(1-e^2)^{1/2}}{s'}\right)$$
$$= [(1-\mu)a]^{1/2}\left[1 + \frac{s}{2s'}e^2 + o(e^4)\right]$$

and (28)

$$\Psi = [(1-\mu)a]^{1/2}\,[1-(1-e^2)^{1/2}]$$
$$= [(1-\mu)a]^{1/2}\left[\frac{e^2}{2s'} + o(e^4)\right].$$

The new Hamiltonian is

$$H' = H + \frac{\partial F}{\partial t} = -\frac{(1-\mu)^2}{2(\Phi - s\Psi)^2} + (s+s')\,\Psi - \Phi - R, \quad (29)$$

where R is to be written in terms of the new variables. In particular,

$$N^{(i,j)} = i\left(\frac{(s+s')\,\varphi + \psi}{s'}\right) + j\left(\frac{\psi + s\varphi}{s'}\right). \quad (30)$$

Note that this new Hamiltonian is explicitly time independent and is thus an integral of the motion. In terms of the Poincaré variables, the resonance condition is

$$\omega_\psi \equiv \frac{\partial}{\partial \Psi}\left(\frac{-(1-\mu)^2}{2(\Phi - s\Psi)^2} + (s+s')\Psi - \Phi - \mu K^{(0,0)}\right) = 0. \quad (31)$$

The term $\mu K^{(0,0)}$ only shifts the position of the resonance by a quantity of order μ and will be ignored in the rest of this paper. The zero-order resonance Hamiltonian must contain all those terms with nearly stationary arguments, i.e., those independent of φ. Inspection of Eq. (30) reveals that the terms independent of φ satisfy

$$js = -i(s+s'), \quad (32)$$

and that for these terms,

$$\cos N^{[is,-i(s+s')]} = \cos i\psi. \quad (33)$$

If we define

$$K_i \equiv K^{[is,-i(s+s')]}, \quad (34)$$

then the zero-order resonance Hamiltonian is

$$H_{ss'}^{(0)} = \frac{-(1-\mu)^2}{2(\Phi - s\Psi)^2} + (s+s')\,\Psi - \Phi - \mu \sum_{i=1}^{\infty} K_i \cos i\psi. \quad (35)$$

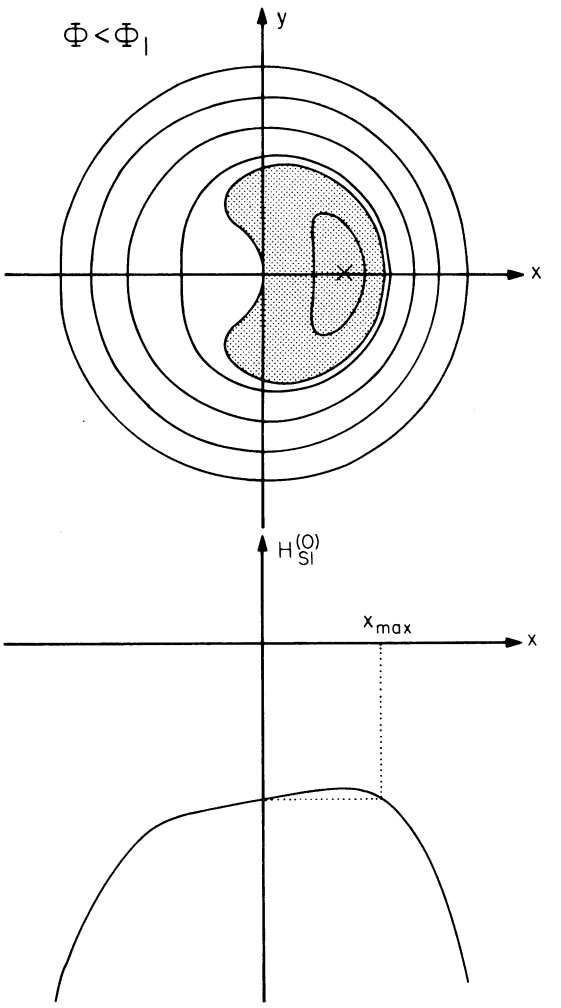

FIG. 2. Contours of constant $H_{s1}^{(0)}$ on a surface of constant Φ for $\Phi < \Phi_1$. The extremum is marked by a cross (×). The region in which Ψ oscillates is shaded. Also shown is a plot of $H_{s1}^{(0)}$ along the x axis which illustrates the definition of x_{max}.

I will be primarily interested in direct motion inside the secondary ($a < 1$) with small eccentricity ($e \leq 0.15$). Because $K_i \propto e^{i|s'|}$ and $s' \geq 1$ when $a < 1$ (see Brouwer and Clemence 1961), the most important resonances are those with $s' = 1$. I will consider only the $s' = 1$ resonances. This greatly simplifies the application of the resonance overlap criterion.

The contours of constant $H_{s1}^{(0)}$ on surfaces of constant Φ have been studied many times (see, for example, Schubart 1964, Message 1966, Jefferys 1966, and Wiesel 1976). Here I will only review the results of these discussions and mention some new features. For a given resonance there are three critical values of Φ which separate qualitatively different types of contours. Figures 2 through 5 illustrate the contours for these four regions. The Cartesian coordinates are $x = (2\Psi)^{1/2}\cos\psi$ and $y = (2\Psi)^{1/2}\sin\psi$. Extrema are marked by a cross (×); points at which contours cross are saddle points. Extrema

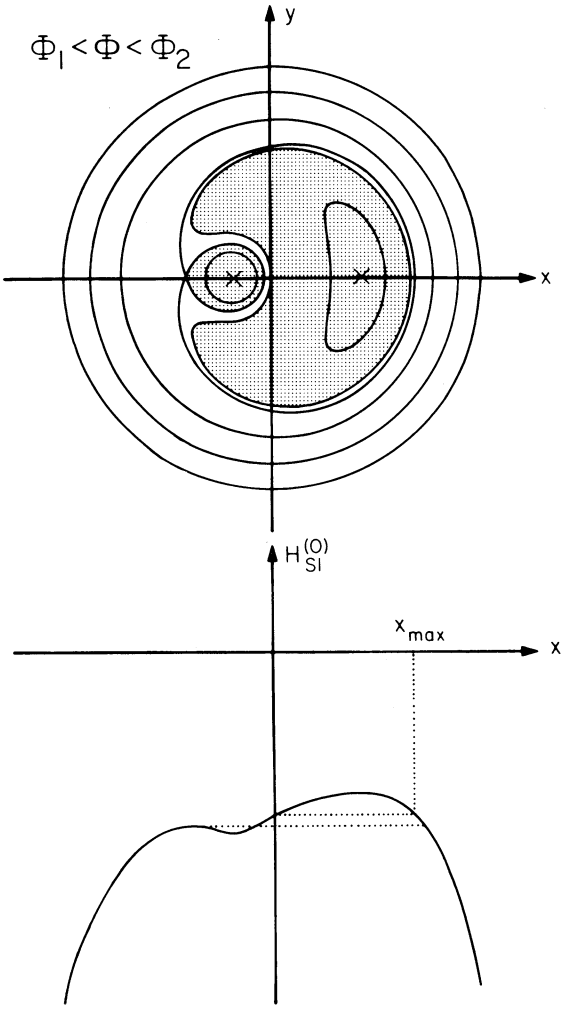

FIG. 3. The same as Fig. 2, but for $\Phi_1 < \Phi < \Phi_2$. There are now two oscillation regions, two extrema, and a saddle point. x_{max} is defined as before.

and saddle points in the zero-order Hamiltonian correspond to stable and unstable periodic orbits, respectively, in the full problem (see Message 1966 for a discussion). Though all the contours are symmetric about $y = 0$, it is not obvious from the form of the Hamiltonian that all the extrema and saddle points lie on the x axis. That this is in fact the case for $a < 1$ was shown by Message (1958). The behavior of the contours is thus completely characterized by plots of $H_{s1}^{(0)}$ along the x axis, which are also illustrated in Figs. 2 through 5. The regions in which ψ oscillates are shaded. For $\Phi < \Phi_1$ there is only one extremum for which $\psi = 0$, and only one oscillation region. The separatrix is that contour which passes through the origin. It crosses the x axis again at $x_{max} = (2\Psi_{max})^{1/2}$, where Ψ_{max} is obviously defined by

$$H_{s1}^{(0)}(\Phi,\Psi = 0) = H_{s1}^{(0)}(\Phi,\Psi_{max},\psi = 0). \quad (36)$$

This is illustrated in Fig. 2. As Φ is increased to Φ_1, a cusp appears which bifurcates into a saddle point and an extremum for $\Phi_1 < \Phi < (1-\mu)^{1/2}$. Φ_1 is near but not identical to Φ_s, which satisfies the modified "resonance condition"

$$0 = \omega_\psi|_{\psi=0} = \frac{-s}{\Phi_s^3} + (s+1). \quad (37)$$

This interval in Φ is further subdivided by Φ_2. Let Ψ_{sp} denote the value of Ψ at the saddle point. The interval $\Phi_1 < \Phi < \Phi_2$ is then characterized by the relation

$$H_{s1}^{(0)}(\Phi,\Psi_{sp},\psi = \pi) < H_{s1}^{(0)}(\Phi,\Psi = 0), \quad (38)$$

and is illustrated in Fig. 3. There are now two oscillation regions. The region that includes $\psi = 0$ is simply a continuation of the oscillation region for $\Phi < \Phi_1$. x_{max} is defined in the same way as before. When Φ is greater than Φ_2, inequality (38) is no longer satisfied and the contours change somewhat (see Fig. 4). The $\psi = 0$ oscillation region now has both an x_{min} and an x_{max}. The

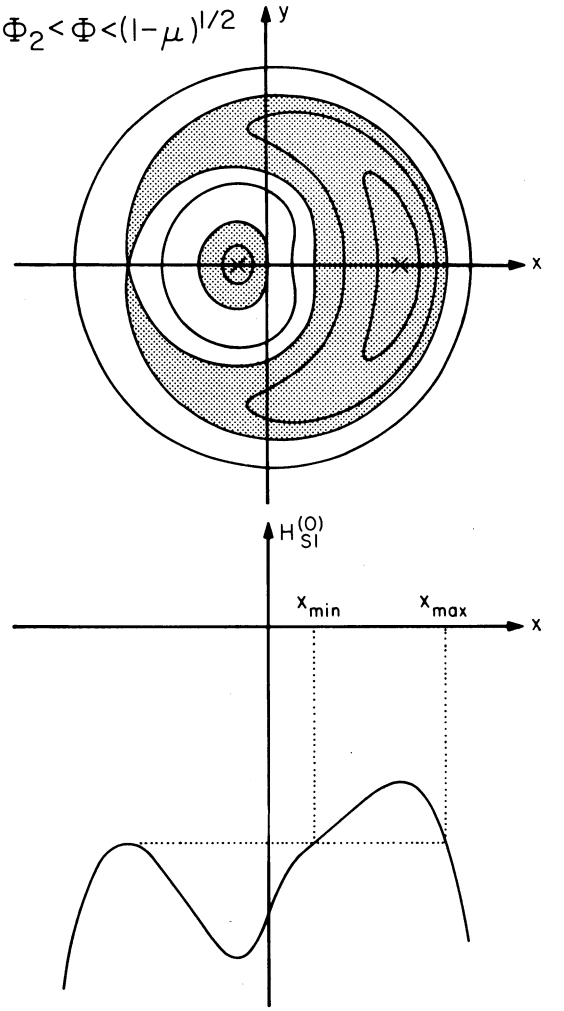

FIG. 4. The same as Figs. 2 and 3, but for $\Phi_2 < \Phi < (1-\mu)^{1/2}$. The oscillation region that includes $\psi = 0$ no longer extends to the origin. The definition of x_{min} is illustrated in the plot of $H_{s1}^{(0)}(y = 0)$ vs x.

contours for $\Phi > (1 - \mu)^{1/2}$ are illustrated in Fig. 5. They are complicated by the appearance of a singularity near the origin. The extremum with $\psi = \pi$ disappears and a new saddle point appears with $\psi = 0$. Near the singularity one does not expect the zero-order Hamiltonian to represent the motion accurately, so this region has been hatched.

The appearance of a new saddle point is quite interesting and has never been mentioned before. As I said above, saddle points correspond to unstable periodic orbits. Thus, this new saddle point corresponds to a new analytic family of periodic orbits in the restricted three-body problem. Colombo *et al.* (1968) have numerically traced out some families of periodic orbits. They found that for some periods there are two periodic orbits, whereas the usual perturbation theory (see, e.g., Message 1966) predicts only one. The appearance of this new family then completes their theoretical explanation. Figure 6 compares the analytic periodic orbits to those found numerically by Colombo *et al.*

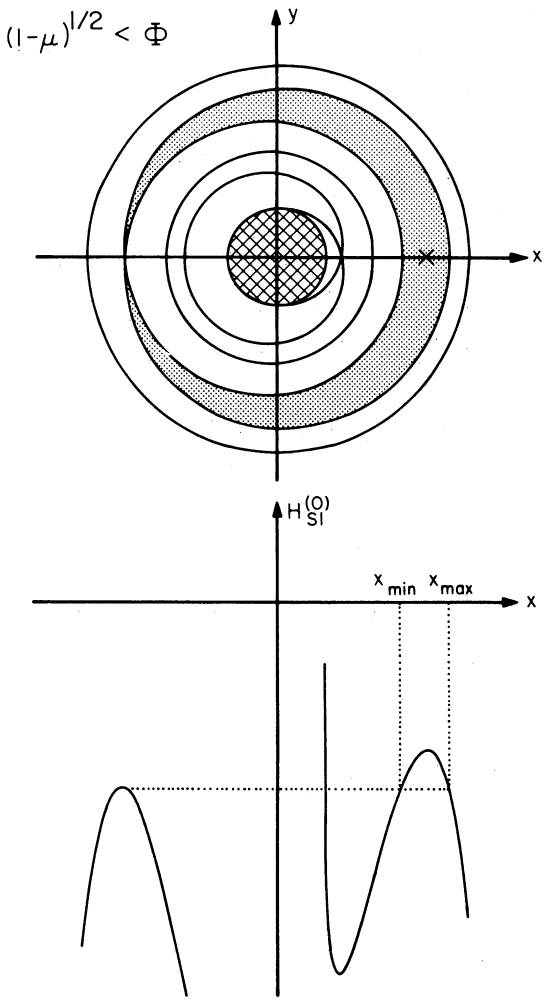

FIG. 5. The same as Figs. 2 through 4, but for $(1 - \mu)^{1/2} < \Phi$. x_{min} and x_{max} are defined as before. There is now a new saddle point with $x > 0$. Near the origin the zero-order resonance Hamiltonian does not represent the motion accurately, so this region has been hatched.

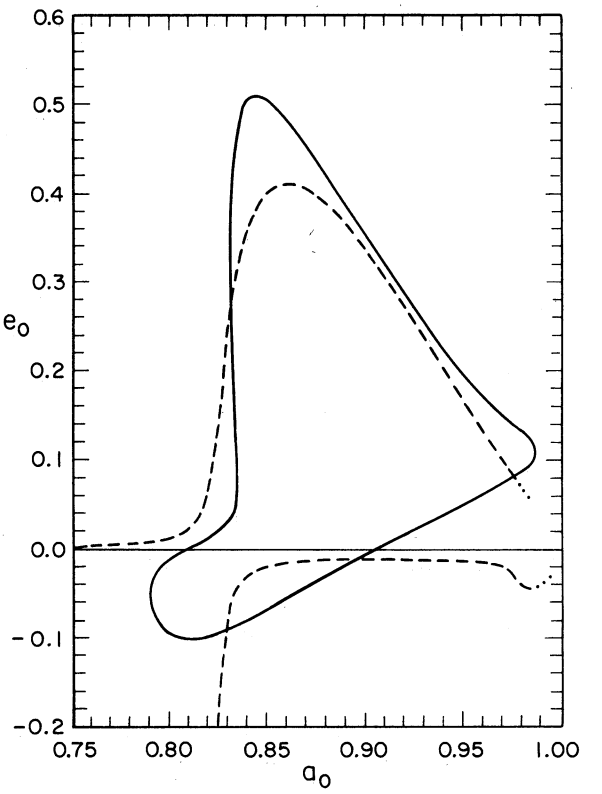

FIG. 6. A comparison of the analytic periodic orbits, including those of the new saddle point, to the periodic orbits found numerically by Colombo *et al.* a_0 and e_0 are the semimajor axis and eccentricity, respectively, at periapse on the line of inferior conjunction.

Rather than study the libration regions in the entire four-dimensional phase space of initial conditions, I restrict my attention to the initial angles $l_0 = 0$ and $g_0 = 0$, i.e., I study the motion of test particles started at periapse on the line of inferior conjunction. It is clearly possible, though, to repeat my analysis for any choice of initial angles. The initial angles $l_0 = g_0 = 0$ are especially easy to analyze since the initial resonance angle ψ_0 is then zero for all resonances. Given particular values of a_0 and e_0, one can calculate Φ_0 and Ψ_0 through Eqs. (28). The test for resonant oscillation when $\psi_0 = 0$ may then be summarized as follows: If $\Phi_0 < \Phi_2$, then ψ oscillates if $\Psi_0 < \Psi_{max}(\Phi_0)$; if $\Phi_0 > \Phi_2$, then ψ oscillates if $\Psi_{min}(\Phi_0) < \Psi_0 < \Psi_{max}(\Phi_0)$. I have used this test to solve numerically for the separatrices in the cases $\mu = 10^{-3}$, 10^{-4}, and 10^{-5}. I kept only the $i = 1$ term in the resonance Hamiltonian (35) and included in it all terms through cubic in the eccentricity (see Brouwer and Clemence 1961). The separatrices of the $s = 3$ and $s = 4$ resonances for $\mu = 10^{-3}$ are plotted in Fig. 7. The combination $1/(a_0^{-3/2} - 1)$ is equal to s when $a_0 = a_{s1}$. The two separatrices for each resonance have been

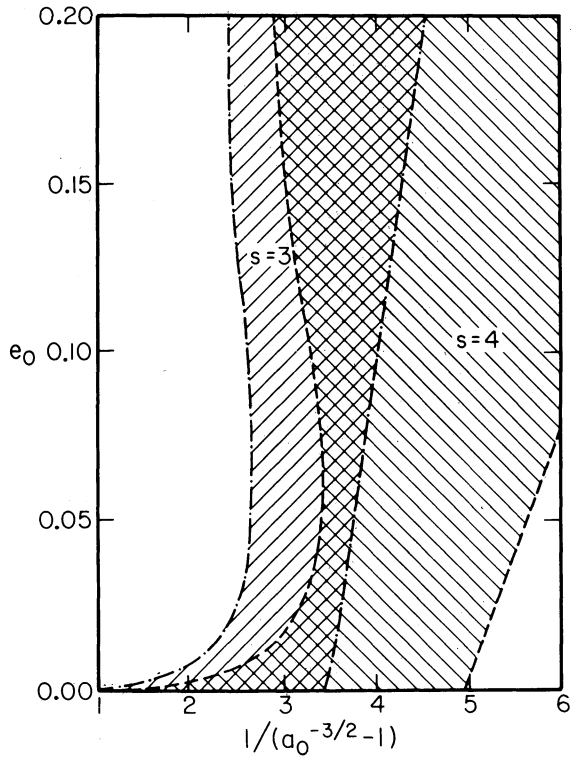

FIG. 7. The oscillation regions of the $s = 3$ and $s = 4$ resonances when $\mu = 10^{-3}$, illustrating the overlap of two resonances. The combination $1/(a_0^{-3/2} - 1)$ is equal to s when $a_0 = a_{s1}$.

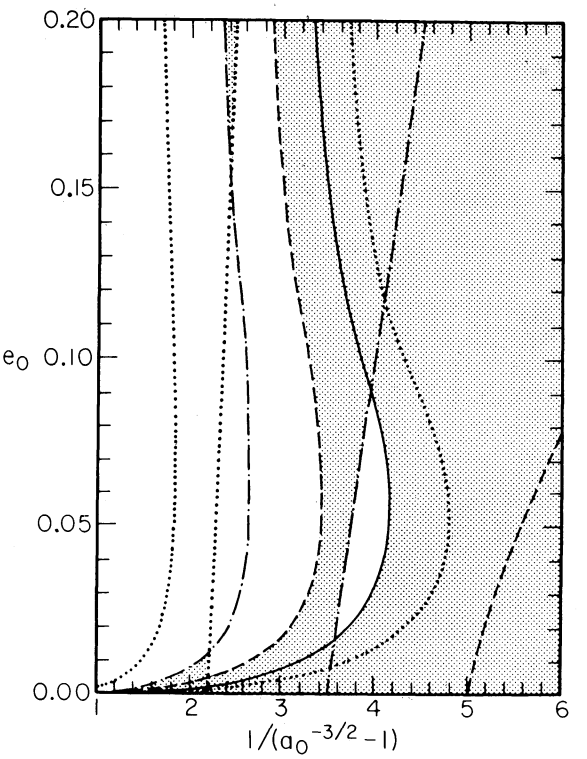

FIG. 8. The oscillation regions for $\mu = 10^{-3}$. The two boundaries of each region are drawn in the same line style. The regions in which two or more resonances overlap are shaded.

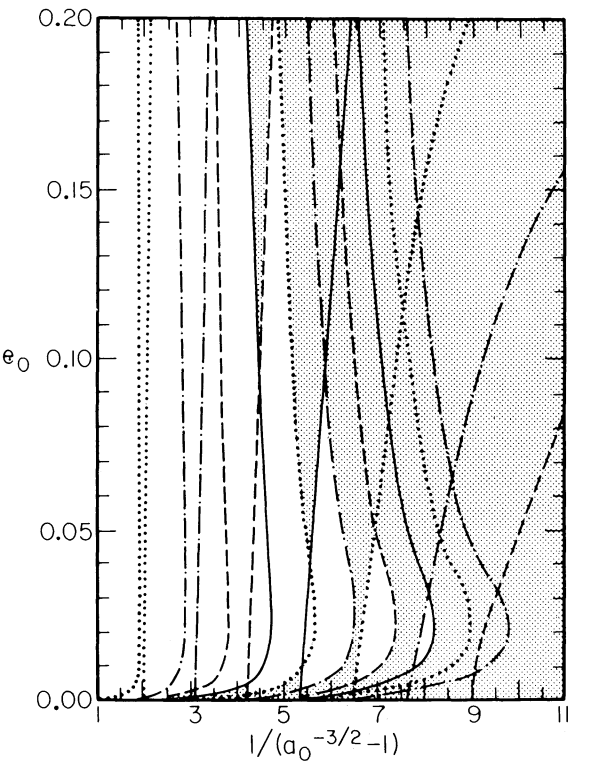

FIG. 9. The same as Fig. 8, but for $\mu = 10^{-4}$.

plotted in the same line style and the oscillation regions are labeled. The overlap of these two resonance oscillation regions is obvious. Figures 8–10 then show the complete diagrams for the secondary masses $\mu = 10^{-3}$, 10^{-4}, and 10^{-5}. While each oscillation region can be found by looking for two nearby lines with the same line style, for clarity only the overlap regions have been shaded. The resonance overlap criterion then predicts that initial conditions chosen from the unshaded regions will lead to quasiperiodic motion and those chosen from the shaded regions will lead to motion with a random character. In Sec. IV, I compare these predictions to some numerical experiments.

IV. EXPONENTIAL SEPARATION AND THE KOMOGOROV-SINAI ENTROPY

There are two numerical tools to determine whether or not motion is quasiperiodic. The most intuitive is the Poincaré surface of section (see Hénon and Heiles 1964). In this method a two-dimensional surface is chosen in the four-dimensional phase space. The equations of motion are then numerically integrated and each crossing of the surface is recorded. If the motion is quasiperiodic, there are two constants of the motion that constrain these crossings to lie on a "simple" curve. If the motion is not quasiperiodic, it is free to roam over some area of the surface. This was the method used by Hénon (1966), Bozis (1966), and Jefferys (1966) in their studies of the

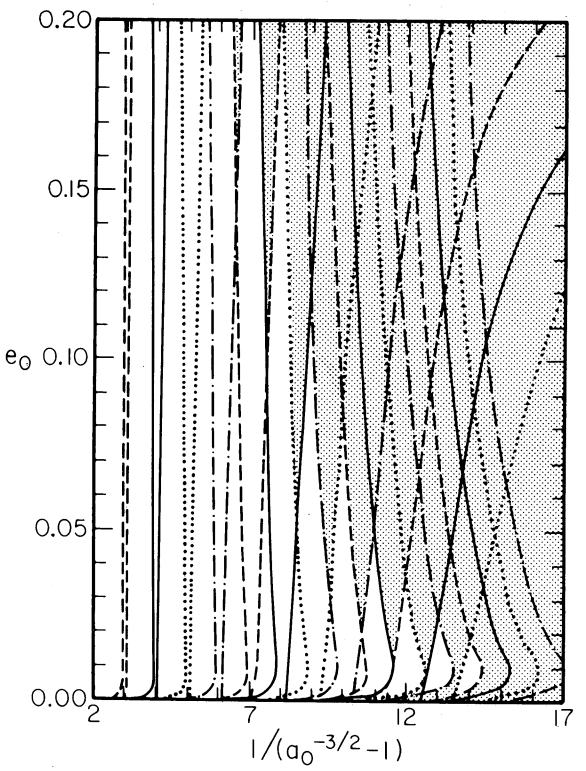

FIG. 10. The same as Figs. 8 and 9, but for $\mu = 10^{-5}$.

restricted three-body problem. This method suffers from the criticism that there is no way to tell whether the crossing points are "random" (i.e., unconstrained) or whether the calculation of more points would reveal that they all lie on a "simple" curve. A more quantitative method, requiring far less computer time, studies the separation of initially nearby orbits with the same value of the (time-independent) Hamiltonian. It has been found (see Chirikov 1979) that in phase space such orbits separate exponentially in the "stochastic" regions and approximately linearly when the motion is quasiperiodic. This is the method I used to study the restricted three-body problem. I examined the separation of nearby orbits for the same secondary masses, $\mu = 10^{-3}$, 10^{-4}, and 10^{-5}, as were studied in Sec. III. I chose the initial eccentricities $e_0 = 0.05$ and $e_0 = 0.10$. Initial semimajor axes a_0 were chosen to span the ranges studied in Sec. III. Of course l_0 and g_0 are zero in all cases. If we consider the system in a rotating frame of reference in which the two masses are stationary, the test particle is started at inferior conjunction with a velocity perpendicular to the line of conjunction. Its partner is also started at inferior conjunction but 10^{-7} closer to the larger mass, with a velocity perpendicular to the line of conjunction chosen so that the values of the Hamiltonian for the two particles are the same. The equations of motion in rotating (synodic) Cartesian coordinates (see Brouwer and Clemence 1961) were then numerically integrated using the algorithm of Bulirasch and Stoer (1966). As is customary for numerical integrations of the restricted problem, the accuracy of the solution was monitored by the variation of the Hamiltonian. In all cases presented here the Hamiltonian never varied by more than $\sim 10^{-10}$ from its initial value and usually varied by only $\sim 10^{-11}$ or 10^{-12}. Figure 11 presents a typical example of what the phase space separation as a function of time looks like in a quasiperiodic regime [$\mu = 10^{-4}$, $e_0 = 0.05$, $1/(a_0^{-3/2} - 1) = 6.5$]. Figure 12 is typical of the exponential separation in a "stochastic" region [$\mu = 10^{-4}$, $e_0 = 0.05$, $1/(a_0^{-3/2} - 1) = 7$]. Note the logarithmic scale in Fig. 12. The rate of divergence can be quantified by fitting in a least-squares sense, the form

$$d(t) = d_0 \exp(h_2 t) \tag{39}$$

to the phase space separation as a function of time, with d_0 equal to the initial separation. This leads to

$$h_2 = \frac{\sum_i t_i \ln(d(t_1)/d_0)}{\sum_i t_i^2} . \tag{40}$$

Every point calculated in each numerical integration up to $t = t_{\max}$ is included in the corresponding sum. The following values of $t_{\max}$ were used: for $\mu = 10^{-3}$, $t_{\max} = 200$; for $\mu = 10^{-4}$, $t_{\max} = 250$; and for $\mu = 10^{-5}$, $t_{\max} = 300$. In an exponential regime, h_2 should be almost independent of $t_{\max}$ (until the separation of the two particles is of order 1), whereas in a linear regime h_2 should decrease approximately as $\ln(t_{\max})/t_{\max}$. The quantity

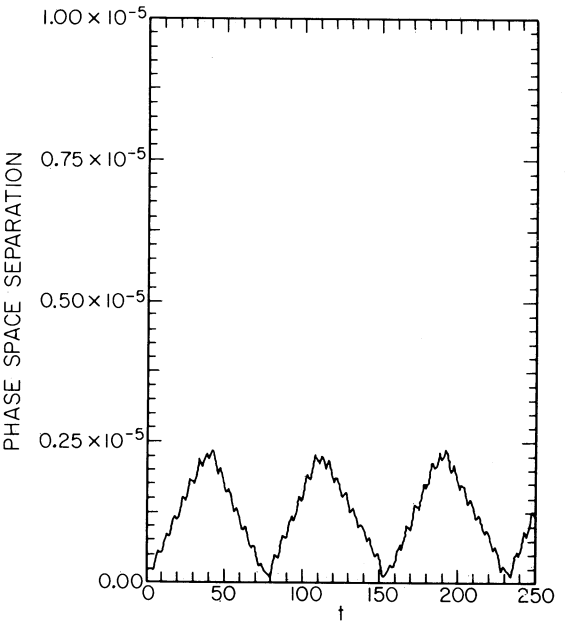

FIG. 11. Typical phase space separation as a function of time in a quasiperiodic regime [$\mu = 10^{-4}$, $e_0 = 0.05$, $1/(a_0^{-3/2} - 1) = 6.5$]. Note the small linear scale on the ordinate.

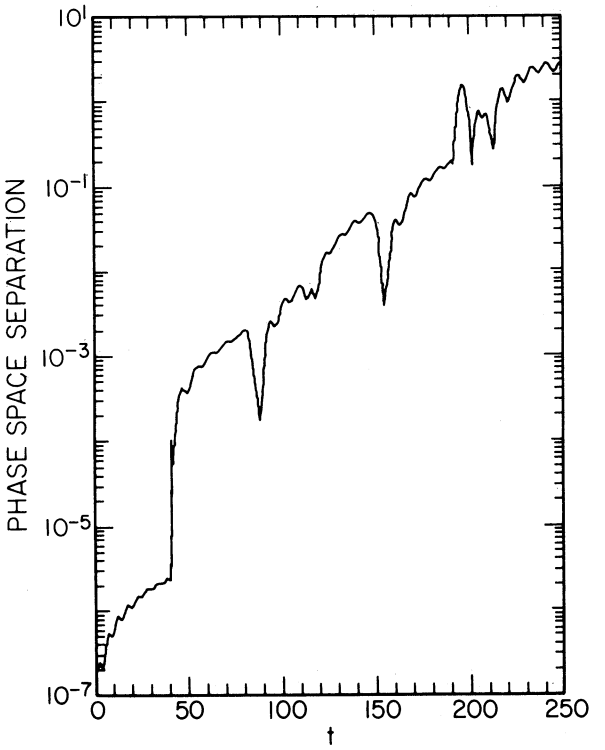

FIG. 12. Typical phase space separation as a function of time in a "stochastic" regime [$\mu = 10^{-4}$, $e_0 = 0.05$, $1/(a_0^{-3/2} - 1) = 7.0$]. Note the logarithmic scale on the ordinate.

h_2 is quite closely related to the Kolmogorov-Sinai entropy h, which is defined by (see Chirikov 1979)

$$h \equiv \left\langle \lim_{d \to 0} \frac{d}{dt} (\ln d) \right\rangle, \tag{41}$$

where the brackets denote an average over the trajectory and $d(t)$ is assumed to be infinitesimal. Figures 13–15 present the results of these calculations. Though the scatter in these plots is fairly large, there is quite clearly a critical value of a_0 in each such that for $a_0 \geq a_{\text{critical}}$, h_2 increases sharply. Figure 16 compares these critical values of a_0 to the predictions of Sec. III. The bars mark the predicted locations of the stochastic instabilities as given by the resonance overlap criterion. The left edge of each bar is the point at which overlap first occurs (for increasing a_0) and the right edge is the point beyond which there is only overlap. In each of the three cases studied, the observed instability occurs within the predicted region. Thus the resonance overlap criterion seems to work very well in the restricted three-body problem. In Sec. V, I derive an approximate criterion for resonance overlap which is valid for all $\mu \ll 1$.

V. SCALING LAW

Though the specific approximations leading to the Chirikov criterion are not valid in the restricted three-body problem, the intuition gained in the numerical study of the separatrices allows us to derive, in the spirit of Chirikov, an approximate criterion for resonance overlap. First, it is clear that no unique widths in semimajor axis can be assigned. For small eccentricity ($e_0 \leq \mu^{1/2}$) the oscillation regions are quite broad and there is overlap at most semimajor axes. For eccentricities greater than $\sim\mu^{1/2}$, the oscillation regions are somewhat more localized in semimajor axis, yet still not uniquely defined. We can characterize the half-widths, though, as the separation of the rightmost ($a_0 > a_{s1}$) boundaries at $e_0 = 0$ from a_{s1}. I call this semimajor axis a_2 since $\Phi(a_2, e_0 = 0) = \Phi_2$. I turn then to the calculation of an approximate expression for Φ_2. Expanding the resonance Hamiltonian (35) about $\Psi = 0$ and retaining only the quadratic terms, one gets

$$H_{s1}^{(0)} \simeq \left(-\frac{1}{2\Phi^2} - \Phi\right) + \left(\frac{-s}{\Phi^3} + (s+1)\right)\Psi + \frac{1}{2}\left(\frac{-3s^2}{\Phi^4}\right)\Psi^2 - \mu K_1 \cos\psi. \tag{42}$$

I have used the fact that for small Ψ (small eccentricity) the sum in Eq. (35) is well approximated by the single

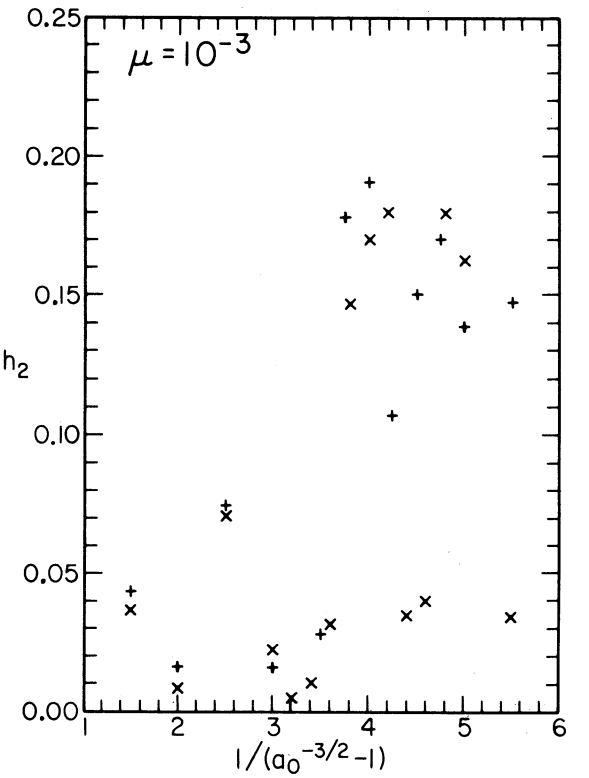

FIG. 13. The entropy h_2 for various initial conditions, with $\mu = 10^{-3}$. Points with initial eccentricity $e_0 = 0.05$ are marked by a cross (×), while points with initial eccentricity $e_0 = 0.10$ are marked by a plus (+).

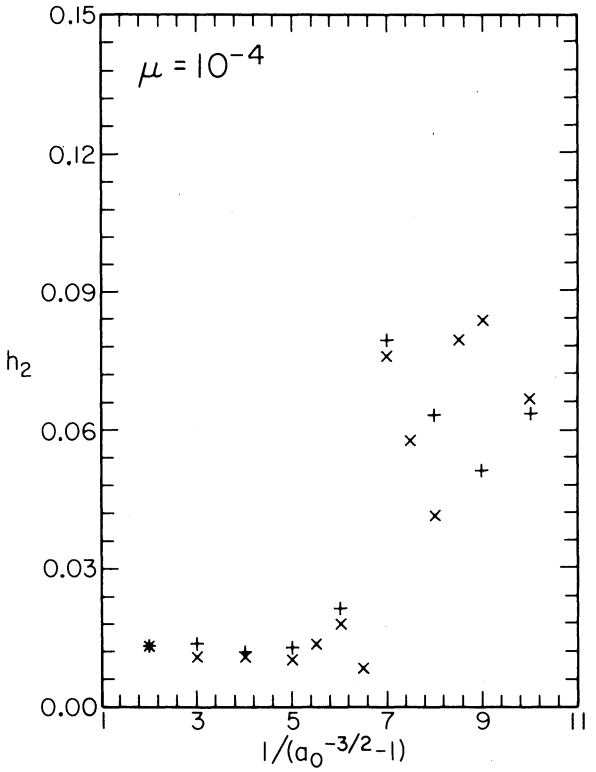

FIG. 14. The same as Fig. 13, but for $\mu = 10^{-4}$.

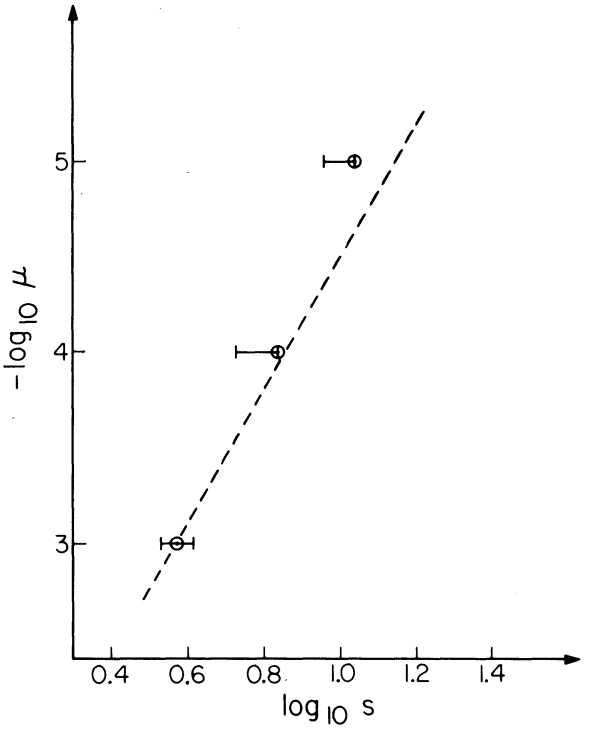

FIG. 16. A comparison of the predictions of the resonance overlap criterion (denoted by horizontal bars) with the location of the observed instability (denoted by a dot with a circle). The dashed line is the approximate theory of Sec. V.

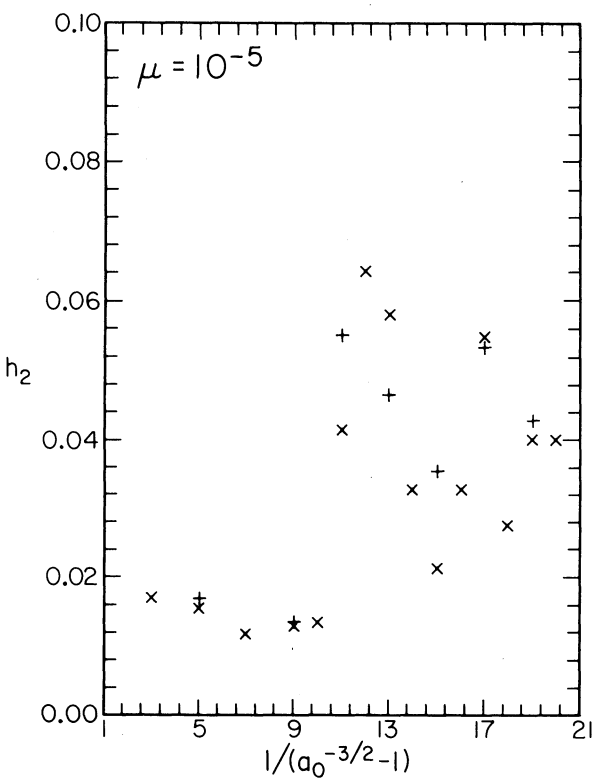

FIG. 15. The same as Figs. 13 and 14, but for $\mu = 10^{-5}$.

term $i = 1$. Further, for sufficiently small Ψ and $\Phi < (1 - \mu)^{1/2}$, K_1 is well approximated by

$$K_1 \simeq (2\Psi)^{1/2} B_s(\Phi, \Psi = 0). \tag{43}$$

Changing to the Cartesian variables $x = (2\Psi)^{1/2} \cos\psi$ and $y = (2\Psi)^{1/2} \sin\psi$, the approximate Hamiltonian (42) becomes, for $y = 0$,

$$H_{s1}^{(0)}(y = 0) \simeq \left(-\frac{1}{2\Phi^2} - \Phi\right) + \left(\frac{-s}{\Phi^3} + (s+1)\right)\frac{x^2}{2} + \frac{1}{2}\left(\frac{-3s^2}{\Phi^4}\right)\frac{x^4}{4} - \mu x B_s(\Phi, \Psi = 0). \tag{44}$$

The extrema of $H_{s1}^{(0)}(y = 0)$ in this approximation can be found by solving the cubic equation

$$0 = \frac{\partial H_{s1}^{(0)}(y = 0)}{\partial x} = \frac{1}{2}\left(\frac{-3s^2}{\Phi^4}\right)x^3 + \left(\frac{-s}{\Phi^3} + (s+1)\right)x - \mu B_s(\Phi, \Psi = 0). \tag{45}$$

First note that for $\Phi < \Phi_1$ there is only one root; thus this Φ_1 approximates the Φ_1 of Sec. III. If we define

$$\delta\Phi_1 \equiv \Phi_1/\Phi_s - 1 \tag{46}$$

and ignore terms of order $\delta\Phi_1$ compared to unity, it is easy to show that for large s,

$$\delta\Phi_1 \simeq (|\mu B_s|)^{2/3} (3/8s)^{1/3}. \tag{47}$$

For a_0 near unity, B_s is well approximated by

$$B_s(a_0) \simeq \frac{-(s+1)}{\pi}\{2K_0[(s+1)(1-a_0)] + K_1[(s+1)(1-a_0)]\}, \quad (48)$$

where K_0 and K_1 are the modified Bessel functions. This expression is evaluated at $a_0 = a_{s1} \simeq 1 - 2/[3(s+1)]$. Equation (47) is then

$$\delta\Phi_1 \simeq 0.62\mu^{2/3} s^{1/3}. \quad (49)$$

This result justifies the statement in Sec. III that Φ_1 is near Φ_s. Φ_2 is determined by the condition

$$H_{s1}^{(0)}(\Phi_2, \Psi_{sp}, \psi = \pi) = H_{s1}^{(0)}(\Phi_2, \Psi = 0), \quad (50)$$

i.e.,

$$0 = \frac{1}{2}\left(\frac{-3s^2}{\Phi_s^4}\right)\frac{x^3}{4} + \frac{3}{2}(s+1)\,\delta\Phi_2\frac{x}{2} - \mu B_s(\Phi_s, \Psi = 0). \quad (51)$$

This equation, along with Eq. (45), allows us to solve for the two unknowns:

$$x_{sp}(\Phi_2) \simeq -1.02\mu^{1/3}s^{-1/3},$$
$$\delta\Phi_2 \simeq 0.79\mu^{2/3}s^{1/3}, \quad (52)$$

where $\Phi_2 = \Phi_s(1 + \delta\Phi_2)$. From the expressions (28) for the Poincaré momenta in terms of the osculating elliptic elements, we see that

$$\Phi \simeq (a_0)^{1/2}(1 + sx^2/2). \quad (53)$$

The half-width of a resonance is then characterized by

$$\delta a_2 \equiv a_2/a_s - 1 \simeq 2\delta\Phi_2. \quad (54)$$

Equating twice this width to the separation of resonances in a_0, which is approximately

$$\Delta a \simeq 2/3s^2, \quad (55)$$

I derive an estimate of when resonances should begin to overlap:

$$s_{overlap} \simeq 0.51\mu^{-2/7}. \quad (56)$$

Equation (56) is plotted in Fig. 13. Since the width of a resonance (in a_0) increases as e_0 increases, Eq. (56) is expected to overestimate $s_{overlap}$.

VI. CONCLUSION

A histogram of the number of asteroids versus semimajor axis (see, for example, Froeschlé and Scholl 1979) reveals a precipitous drop in the number of asteroids with semimajor axes outside the 2/1 resonance. This fact led Lecar and Franklin (1973) to hypothesize a dynamical origin for the absence of asteroids in this region. To test their hypothesis they integrated 260 test objects distributed uniformly between $0.55a_J$ and $0.85a_J$, where a_J is Jupiter's semimajor axis, with eccentricities between 0.0 and 0.3. They found that objects started exterior to $0.85a_J$ were "ejected" immediately and that within the 200 Jupiter revolution time span of their integrations, the region outside the 3/2 resonance was cleared, except for some objects at the 4/3 resonance. The region between the 2/1 resonance and the 3/2 resonance, however, remained well populated. They suggested that longer integrations might deplete this region. To test this hypothesis Froeschlé and Scholl (1979) performed a similar experiment covering a time span of 10^5 yr. The region was still not sufficiently depleted. In addition they found that after 60000 yr no more objects escaped. Since the secular perturbations of the planets cause variations in the orbital elements with time scales of order 10^5 yr or longer (see Brouwer and van Woerkem 1950), it may be necessary to extend these numerical experiments to several million years before they capture all the dynamical features that are present. The extension of these calculations to much longer times, though, appears to be prohibitively expensive. Even if their numerical experiments had depleted the region outside the 2/1 resonance, we would have wanted a qualitative understanding of those dynamical features which led to the instability. The failure of the numerical experiments and the cost of extending them to the required time span heightens the need for a qualitative understanding of the instabilities in asteroidal motion. This paper constitutes a first step towards this qualitative understanding. I have applied the resonance overlap criterion to the planar circular-restricted three-body problem and compared its predictions to some numerical experiments. Since the predictions are in remarkably good agreement with my numerical experiments, great confidence has been gained in the usefulness of the resonance overlap criterion for obtaining a qualitative understanding of the instabilities in the solar system.

It is a pleasure to thank Peter Goldreich for valuable advice and helpful criticism. This work was partially supported by NASA Grant NGL 05-002-003.

REFERENCES

Bozis, G. (1966). Astron. J. **71**, 404.
Brouwer, D., and van Woerkom, A. J. J. (1950). Astron. Papers of the American Eph. **13**, 81.
Brouwer, D., and Clemence, G. M. (1961). *Methods of Celestial Mechanics* (Academic, New York).
Bulirasch, R., and Stoer, J. (1966). Numerische Math. **8**, 1.
Chirikov, B. V. (1979). Phys. Rep. **52**, 263.
Colombo, G., Franklin, F. A., and Munford, C. M. (1968). Astron. J. **73**, 111.
Froeschlé, C., and Scholl, H. (1979). Astron. Astrophys. **72**, 246.
Hagihara, Y. (1943). Jpn. J. Astron. Geophys. **21**, 29.
Hénon, M., and Heiles, C. (1964). Astron. J. **69**, 73.
Hénon, M. (1966). *The Theory of Orbits in the Solar System and in Stellar Systems*, IAU Symposium No. 25 (Academic, London),

p. 157.
Jefferys, W. H. (1966). Astron. J. **71,** 306.
Lecar, M., and Franklin, F. (1973). Icarus **73,** 422.
Message, P. J. (1958). Astron. J. **63,** 443.
Message, P. J. (1966). *The Theory of Orbits in the Solar System and in Stellar Systems,* IAU Symposium No. 25 (Academic, London), p. 197.
Moser, J. (1973). *Stable and Random Motions in Dynamical Systems* (Princeton University, Princeton, N.J.).
Poincaré, H. (1902). Bull. Astron. **19,** 289.
Schubart, J. (1964). Smithsonian Astrophys. Obs. Spec. Rep. No. 149.
Walker, G. H., and Ford, J. (1969). Phys. Rev. **188,** 416.
Whittaker, E. T. (1961). *A Treatise on the Analytical Dynamics of Particles and Rigid Bodies,* 4th ed. (Cambridge University, Cambridge, England).
Wiesel, W. E. (1976). Celestial Mech. **13,** 3.
Woltjer, J. (1923). Bull. Astron. Inst. Neth. **1,** 219.